Article:
Keller, D, Buecheler, S, Reinhard, P et al. (2016) Band gap widening at random CIGS grain boundary detected by valence electron energy loss spectroscopy. Applied Physics Letters, 109 (15). 153103. ISSN: 0003-6951

https://doi.org/10.1063/1.4964516

Band gap widening at random CIGS grain boundary detected by valence electron energy loss spectroscopy

Cite as: Appl. Phys. Lett. **109**, 153103 (2016); https://doi.org/10.1063/1.4964516
Submitted: 12 August 2016 . Accepted: 27 September 2016 . Published Online: 10 October 2016

Debora Keller, Stephan Buecheler, Patrick Reinhard, Fabian Pianezzi, Benjamin Bissig, Romain Carron, Fredrik Hage, Quentin Ramasse, Rolf Erni, and Ayodhya N. Tiwari

Band gap widening at random CIGS grain boundary detected by valence electron energy loss spectroscopy

Debora Keller,[1,2,a)] Stephan Buecheler,[1] Patrick Reinhard,[1] Fabian Pianezzi,[1] Benjamin Bissig,[1] Romain Carron,[1] Fredrik Hage,[3] Quentin Ramasse,[3] Rolf Erni,[2] and Ayodhya N. Tiwari[1]

[1]*Laboratory for Thin Films and Photovoltaics, Empa - Swiss Federal Laboratories for Materials Science and Technology, Ueberlandstrasse 129, CH-8600 Duebendorf, Switzerland*
[2]*Electron Microscopy Center, Empa - Swiss Federal Laboratories for Materials Science and Technology, Ueberlandstrasse 129, CH-8600 Duebendorf, Switzerland*
[3]*SuperSTEM Laboratory, SciTech Daresbury Campus, Keckwick Lane, Daresbury WA4 4AD, United Kingdom*

(Received 12 August 2016; accepted 27 September 2016; published online 10 October 2016)

Cu(In,Ga) Se_2 (CIGS) thin film solar cells have demonstrated very high efficiencies, but still the role of nanoscale inhomogeneities in CIGS and their impact on the solar cell performance are not yet clearly understood. Due to the polycrystalline structure of CIGS, grain boundaries are very common structural defects that are also accompanied by compositional variations. In this work, we apply valence electron energy loss spectroscopy in scanning transmission electron microscopy to study the local band gap energy at a grain boundary in the CIGS absorber layer. Based on this example, we demonstrate the capabilities of a 2nd generation monochromator that provides a very high energy resolution and allows for directly relating the chemical composition and the band gap energy across the grain boundary. A band gap widening of about 20 meV is observed at the grain boundary. Furthermore, the compositional analysis by core-loss EELS reveals an enrichment of In together with a Cu, Ga and Se depletion at the same area. The experimentally obtained results can therefore be well explained by the presence of a valence band barrier at the grain boundary. *Published by AIP Publishing*. [http://dx.doi.org/10.1063/1.4964516]

Cu(In,Ga)Se_2 (CIGS) thin film solar cells show a promising potential for the development of highly efficient, low-cost solar cells. Efficiencies of up to 22.3% have been reached,[1] but nevertheless many fundamental material properties governing the performance are still not clearly understood. The polycrystalline structure of CIGS and the compositional inhomogeneities influence the local electronic properties of the absorber layer and affect the charge carrier transport. Grain boundaries represent the most common structural defect type in CIGS and were widely studied in the past, leading to different insights into the local chemistry and geometry of different grain boundary types. Regarding the composition of random grain boundaries, both an increase in the Cu concentration, combined with a decrease of the Se and In concentrations, and the exact opposite case have been reported. Often, an enrichment of impurity atoms (such as O, K and Na) at the grain boundaries was observed in parallel (see e.g., Refs. 2–4). Therefore, no clearly dominant grain boundary model has been found that would explain all the findings and could generally predict the electronic properties at the CIGS grain boundaries. Instead, the local structural and compositional properties vary depending on the analyzed grain boundary. It is commonly believed that the grain boundaries in CIGS are benign, but the interruption of the crystal lattice and the compositional variations may still affect the electronic properties in different ways. Therefore, a clearer understanding on how the nanoscale inhomogeneities at grain boundaries influence the electronic loss mechanisms in CIGS would be highly beneficial to further improve the solar cell performance in a targeted way. Valence electron energy loss spectroscopy (VEELS) is a transmission electron microscopy (TEM) based technique that allows for characterizing electronic properties at the nanometer scale. It is a very promising tool for the analysis of, e.g., the local band gap energy (E_g) in CIGS solar cells.[5] However, the high energy resolution, which is required to access the 1.0 eV to 1.7 eV band gap energy of CIGS, challenges the limits of the current state-of-the-art electron sources. This work demonstrates the ability of a 2nd generation monochromator, which provides very high energy resolution (40 meV in the present work), to study the local band gap variations in CIGS and directly relate the results to the local composition.

The investigated CIGS absorber layer was produced following the low-temperature co-evaporation process for high efficiency solar cells on flexible polyimide foils, as described by Chirilă *et al.*, yielding CIGS absorbers with a Ga compositional grading along the depth.[6,7] An NaF and KF post-deposition treatment was used for the samples in this study. The average composition of the absorber layer was determined by X-ray fluorescence (XRF), revealing a [Ga]/([Ga] + [In]) ratio (GGI) of 0.34 and a [Cu]/([Ga] + [In]) ratio (CGI) of 0.78. As the investigated grain boundary was in the Ga-notch region, the GGI is expected to be lower there (GGI ~ 0.2), compared to the average GGI. This corresponds to a band gap energy of about 1.1 eV. The TEM specimens were prepared by conventional cross-section polishing, and subsequent Ar^+-ion milling until electron transparency was

a)debora.keller@empa.ch

reached. This was done on a Fischione TEM ion mill 1050 that provided liquid N_2 cooling to prevent the specimen from overheating during the milling process.

The Nion UltraSTEM 100MC HERMES installed at the SuperSTEM laboratory (UK) was used for the VEELS experiments. The instrument is equipped with a cold field emission gun (cFEG) and a high-energy-resolution monochromator, and it was operated at 100 kV. In order to improve the signal-to-noise ratio (SNR), the spectra were recorded in the DualEELS mode: The low-loss region was recorded within the energy frame of 0.27 eV to 20.75 eV at a dispersion of 10 meV per pixel with an acquisition time of 500 ms and the zero-loss peak (ZLP) was recorded within the energy frame of −1.94 eV to 18.46 eV at a dispersion of 10 meV per pixel for 5 ms. At these settings, the full with at half maximum (FWHM) of the ZLP was 40 meV. The band gap was extracted from the low-loss spectrum according the procedure depicted in Figure 1. The contribution of the ZLP was subtracted from the raw spectra by fitting a power-law function to the descending tail. The optimal fit range (0.95 eV to 1.10 eV) was defined based on the statistical and visual evaluation of the results, which were obtained after applying different ranges. Using this fit range allowed for minimizing artifacts such as negative intensities or loss of relevant intensities. However, the final choice of the boundaries as long as they were chosen in a reasonable range did not significantly affect the resulting relative band gap variation. Then, the band gap energy was determined by fitting a parabola to the remaining spectrum, as described in more detail by Keller *et al.*[5] The parabola was fitted based on the energy range 1.5 eV to 1.9 eV after careful evaluation of the optimal range. This optimal range was determined within the region, where small changes in the fitting range did not lead to significantly different results. Whereas the absolute values of the obtained band gap energies were shifted as a function of the energy range chosen for fitting, the relative band gap variation did not change significantly. However, the shape of the onset is assumed to follow a parabolic shape down to the onset. If this condition is not fulfilled, then the estimated absolute value of the band gap energy that is obtained by extrapolation from the fit region is not reliable (see e.g., Refs. 5 and 8).

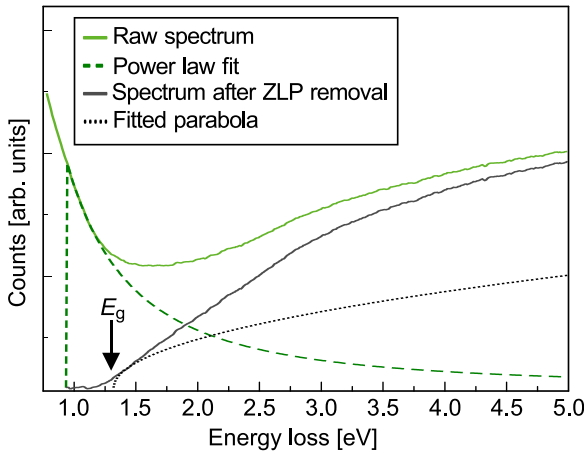

FIG. 1. Band gap extraction procedure from a raw VEEL spectrum. The contribution of the ZLP was approximated by a power-law fit and subsequently subtracted. Then, a parabola was fitted to the remaining spectrum, whereas the onset of the parabola was defined as the band gap energy.

The core-loss EELS data were recorded by the same instrument using a dispersion of 1 eV per pixel and an acquisition time of 0.35 s. A principle component analysis was used to reduce noise in the EEL spectra. The relative spatial distributions were estimated based on the L-edge of Cu at 931 eV, the M-edge of In at 443 eV, the L-edge of Ga at 1115 eV and the L-edge of Se at 1436 eV. To obtain the spatial distribution maps of the different elements, the decaying background was first subtracted using a power-law fit and subsequently the intensities of the relevant EELS edges were integrated. The considered energy ranges were 388 eV to 415 eV (background) and 441 eV to 602 eV (edge) for the In distribution, 795 eV to 881 eV (background) and 896 eV to 1198 eV (edge) for the Cu distribution, 1015 eV to 1072 eV (background) and 1100 eV to 1182 eV (edge) for the Ga distribution, and 1344 eV to 1370 eV (background) and 1395 eV to 1698 eV (edge) for the Se distribution.

Four VEELS profiles were acquired across a random grain boundary, as indicated in the high-angle annular dark field (HAADF) image in Figure 2(a). The profiles 1–3 all revealed a similar, non-negligible increase in the band gap energy at the grain boundary, while profile 4 did not reveal a significant band gap fluctuation. In order to estimate the average relative increase in the band gap energy at the grain boundary, only the profiles 1–3 were considered. For those, the band gap energy was evaluated within the 40 nm distance across the grain boundary in 5 nm sized steps, as indicated by the white boxes in Figure 2(a). Then, the band gap variation across the grain boundary (Figure 2(b)) was determined as an average of profiles 1–3, considering the 7 steps indicated by the white boxes (Figure 2(a)). According to this evaluation, the band gap energy increases by around 20 meV at the grain boundary. The error bars take into account the uncertainty due to (i) the limited acquisition reproducibility, i.e., the deviation between the profiles 1–3; (ii) the choice of the energy range considered for ZLP fitting and subtraction (three ranges considered: 0.90 eV to 1.05 eV, 0.95 eV to 1.10 eV and 0.99 eV to 1.15 eV); and (iii) the choice of the energy range considered for fitting the parabola to extract the band gap energy (four ranges considered: 1.4 eV to 1.8 eV, 1.5 eV to 1.9 eV, 1.6 eV to 2.0 eV and 1.4 eV to 2.0 eV). Even by using a state-of-the-art STEM with unique energy resolution, the error bars are still rather large to reliably measure band gap shifts of 20 meV.

The core-loss EELS maps were recorded within the area marked by the yellow box in Figure 2(a). The elemental distribution maps of Cu, In, Ga and Se are shown in Figure 2(c) and the corresponding profiles (averaged over the map width) in (d). An In enrichment and depletion of Cu, Se and Ga are observed at the grain boundary. Furthermore, an additional variation of the In, Ga and Cu distribution is present in the middle of the grain boundary, i.e., the Cu and In concentrations decrease, whereas the Ga concentration rises slightly (Figure 2(d)).

Different models for describing the electronic properties at grain boundaries in CIGS have been proposed in the literature (e.g., Refs. 9 and 10). These consider different elemental distributions of the main elements Cu, In, Ga, and Se at the

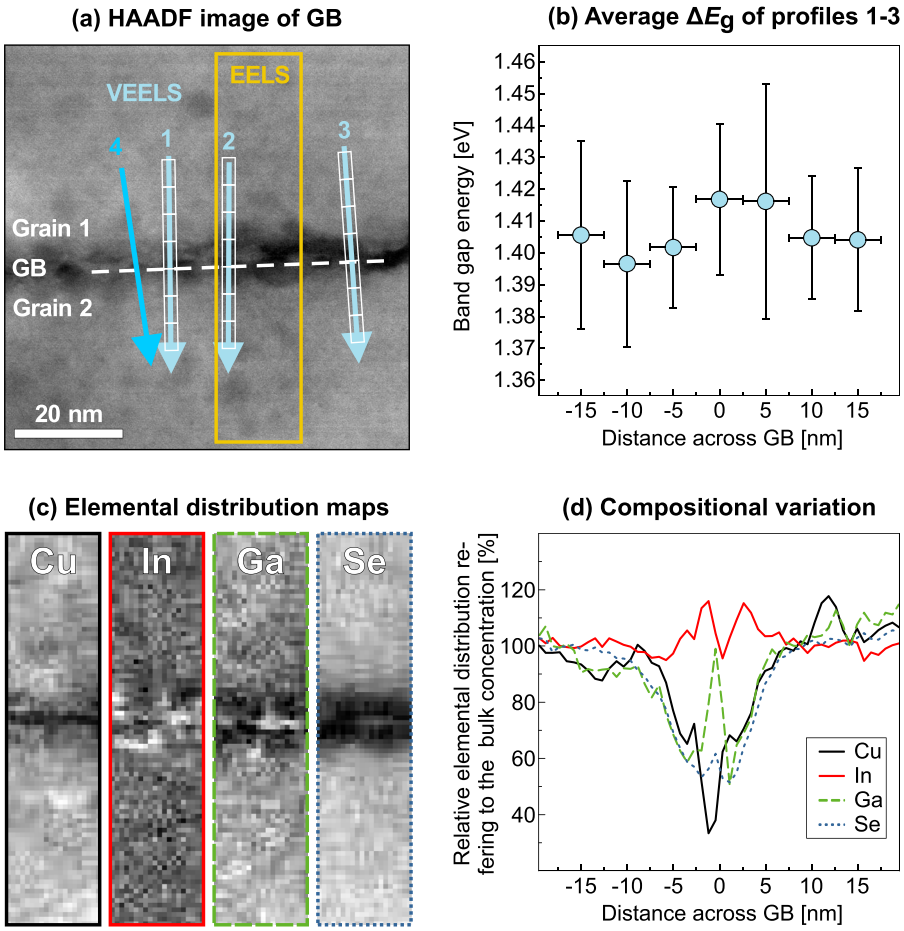

FIG. 2. Band gap variation and elemental distribution at a random grain boundary. (a) HAADF image of the analyzed grain boundary. The regions where VEELS line profiles and core-loss EELS maps were acquired are indicated by the blue lines resp. the yellow box. (b) Band gap variation measured across the grain boundary as an average of the data recorded along the lines 1–3. (c) Relative, spatial distribution maps of Cu, In, Ga and Se recorded by EELS within the yellow box marked in (a). (d) Compositional variation across the grain boundary extracted from the elemental maps shown in (c). The concentration of each element is described as a percentage of the bulk reference value, which is defined as the concentration at ~10 nm to 20 nm distance to the grain boundary.

grain boundary as well as the presence of bound charges due to impurity atoms and dangling bonds (Figure 3). The presence of bound charges results in parallel fluctuation of the band edges (band bending), which does not affect the band gap energy (Figure 3(a)). In contrast, the relative variation of the main element concentrations affects the band gap energy. The valence band maximum (E_V) is determined by the Cu 3d and Se 4p antibonding states, and therefore Cu depletion lowers the valence band maximum.[8,11,12] The conduction band minimum (E_C) strongly depends on the GGI present: increasing Ga concentration shifts the conduction band minimum towards higher energies.[8,12–14] Regarding the three models, the measured band gap widening at the grain

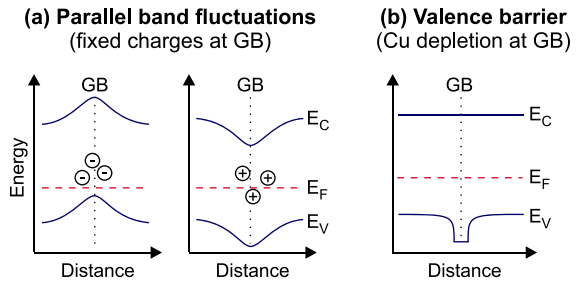

FIG. 3. Different models of the band structure at a CIGS grain boundary. Charges that are bound to the grain boundary cause parallel fluctuations of the band edges and do not result in detectable band gap fluctuations (a). In contrast, the model describing a valence band barrier (b) causes a band gap widening, which agrees well with our experimental results. However, a combination of the valence band barrier and parallel band bendings cannot be excluded.

boundary can be explained by the valence band barrier model (Figure 3(b)), which is also in agreement with the coincident Cu depletion. Alternatively, a combination of models resulting in additional parallel band edge fluctuations cannot be excluded. For CIGS, valence band bendings of up to 100 meV have been suggested in the literature.[9,15] This is significantly more than the experimentally observed variation of 20 meV in this study. In fact, the measured band gap fluctuation derived by VEELS might be underestimated. Firstly, delocalization effects and the chosen step size of 5 nm blur the spatial resolution, which dampens the experimentally detectable change of the band gap energy.[16] And secondly, data processing (the parabolic fit) generally detects the smallest band gap present in the investigated volume. Since the grain boundary is a random one, it is well possible that the investigated volume contains overlapping contributions from the grains and the grain boundary. The VEELS measurement would then very likely reveal the lower band gap present in the grain and not the higher band gap of the grain boundary. This effect can also explain why no band gap fluctuation was observed along the profile 4 (Figure 2(a)). Furthermore, it could be responsible for the apparent local shift between the band gap variation (Figure 2(b)) and the compositional variation (Figure 2(d)) that were measured. According to the literature, it is expected that Cu depletion causes a downward bending of the valence band that could explain the observed band gap widening at the grain boundary.[8] However, in the present specimens, the actual energy changes of the valence band due to

compositional variations still need to be determined. In general, the downwards bending of the valence band at the grain boundary and the related valence barrier are supposed to repel the holes from the grain boundary. Consequently, charge carrier recombination is hampered, which provides a possible explanation for the generally benign nature of grain boundaries in CIGS.

In summary, the purpose of the present work is to exemplarily show the applicability of state-of-the-art electron microscopy analytics to measure the band gap variations very locally in CIGS. The local electronic properties and composition at a random CIGS grain boundary were therefore studied by (V)EELS using a 2nd generation monochromator. A small but significant band gap widening at the grain boundary was observed by fitting the VEELS data. The measured band gap widening is roughly 20 meV; however, due to experimental and physical limitations, the actual band gap widening is likely to be underestimated in these first experiments. Core-loss EELS was used to provide information about the local composition, which revealed local In enrichment and depletion of Cu, Ga and Se at the grain boundary. A band gap widening combined with Cu depletion indicates the presence of a valence band barrier at the grain boundary. As a consequence of such a barrier, the holes would be repelled from the grain boundary and the charge carrier recombination would be reduced at the grain boundary.

The financial support from the Swiss National Science Foundation (SNF) (Project No. 200020_132377) and the UK National Facility for Aberration-Corrected STEM, supported by the Engineering and Physical Scences Research Council (EPSRC), are greatly acknowledged.

[1]See http://www.solar-frontier.com/eng/news/2015/C051171.html for "Solar frontier achieves world record thin-film solar cell efficiency: 22.3%," (last accessed December 15, 2015).
[2]P.-P. Choi, O. Cojocaru-Mirédin, R. Wuerz, and D. Raabe, J. Appl. Phys. **110**, 124513 (2011).
[3]D. Abou-Ras, B. Schaffer, M. Schaffer, S. S. Schmidt, R. Caballero, and T. Unold, Phys. Rev. Lett. **108**, 075502 (2012).
[4]O. Cojocaru-Mirédin, P.-P. Choi, D. Abou-Ras, S. Schmidt, R. Caballero, and D. Raabe, IEEE J. Photovoltaics **1**, 207 (2011).
[5]D. Keller, S. Buecheler, P. Reinhard, F. Pianezzi, D. Pohl, A. Surrey, B. Rellinghaus, R. Erni, and A. N. Tiwari, Microsc. Microanal. **20**, 1246 (2014).
[6]A. Chirilă, S. Buecheler, F. Pianezzi, P. Bloesch, C. Gretener, A. R. Uhl, C. Fella, L. Kranz, J. Perrenoud, S. Seyrling, R. Verma, S. Nishiwaki, Y. E. Romanyuk, G. Bilger, and A. N. Tiwari, Nat. Mater. **10**, 857 (2011).
[7]A. Chirilă, P. Reinhard, F. Pianezzi, P. Bloesch, A. R. Uhl, C. Fella, L. Kranz, D. Keller, C. Gretener, H. Hagendorfer, D. Jaeger, R. Erni, S. Nishiwaki, S. Buecheler, and A. N. Tiwari, Nat. Mater. **12**, 1107 (2013).
[8]S. Minoura, K. Kodera, T. Maekawa, K. Miyazaki, S. Niki, and H. Fujiwara, J. Appl. Phys. **113**, 063505 (2013).
[9]S. Siebentritt, M. Igalson, C. Persson, and S. Lany, Prog. Photovoltaics **18**, 390 (2010).
[10]T. Unold and C. A. Kaufmann, in *Comprehensive Renewable Energy*, edited by A. Sayigh (Elsevier, Oxford, 2012), pp. 399–422.
[11]S.-H. Han, F. S. Hasoon, J. W. Pankow, A. M. Hermann, and D. H. Levi, Appl. Phys. Lett. **87**, 151904 (2005).
[12]S. Minoura, T. Maekawa, K. Kodera, A. Nakane, S. Niki, and H. Fujiwara, J. Appl. Phys. **117**, 195703 (2015).
[13]S.-H. Wei, S. B. Zhang, and A. Zunger, Appl. Phys. Lett. **72**, 3199 (1998).
[14]P. D. Paulson, R. W. Birkmire, and W. N. Shafarman, J. Appl. Phys. **94**, 879 (2003).
[15]J. H. Werner, J. Mattheis, and U. Rau, in *Thin Solid Films EMRS 2004 Proceedings of Symposium O on Thin Film Chalcogenide Photovoltaic Materials, EMRS 2004 Conference, Strasbourg, France, May 24–28, 2004* (2005), Vol. 480–481, p. 399.
[16]R. Egerton, *Electron Energy-Loss Spectroscopy in the Electron Microscope* (Springer US, Boston, MA, 2011).